



## Impact pressure of debris flow on beam dam

Dong-wei WANG, Yong YOU, Jin-feng LIU, Hao SUN, Zhuang WANG

View online: <https://doi.org/10.1007/s10346-018-1065-2>

---

### Articles you may be interested in

[Characteristics of debris flow impact on a double-row slit dam](#)

Journal of Mountain Science. 2023, 20(2): 415 <https://doi.org/10.1007/s11629-022-7462-y>

[Dynamic response analysis of blocks-combined dam under impact load](#)

Journal of Mountain Science. 2020, 17(11): 2827 <https://doi.org/10.1007/s11629-019-5619-0>

[Experimental study on characteristics of trapping and regulating sediment with an open-type check dam in debris flow hazard mitigation](#)

Journal of Mountain Science. 2018, 15(9): 2001 <https://doi.org/10.1007/s11629-017-4619-1>

[The siltation of debris flow behind check dam in the midstream of Bailong River](#)


Journal of Mountain Science. 2018, 15(1): 100 <https://doi.org/10.1007/s11629-017-4484-y>



[A debris-flow impact pressure model combining material characteristics and flow dynamic parameters](#)


Journal of Mountain Science. 2018, 15(12): 2721 <https://doi.org/10.1007/s11629-018-5114-z>


Original Article


## Impact pressure of debris flow on beam dam

**WANG Dong-wei**<sup>1,2,3</sup>  <https://orcid.org/0000-0001-6189-8721>; e-mail: wangdongwei@imde.ac.cn

**YOU Yong**<sup>1,2\*</sup>  <http://orcid.org/0000-0001-7863-8686>;  e-mail: yyong@imde.ac.cn

**LIU Jin-feng**<sup>1,2</sup>  <http://orcid.org/0000-0002-5542-827X>; e-mail: liujf@imde.ac.cn

**SUN Hao**<sup>1,2</sup>  <http://orcid.org/0000-0001-9300-5553>; e-mail: sunhao@imde.ac.cn

**WANG Zhuang**<sup>1,2,3</sup>  <https://orcid.org/0000-0001-7900-0457>; e-mail: zhuangwang@imde.ac.cn

\*Corresponding author

<sup>1</sup> Key Laboratory of Mountain Hazards and Earth Surface Process, Chinese Academy of Sciences, Chengdu 610041 China

<sup>2</sup> Institute of Mountain Hazards and Environment, CAS, Chengdu 610041, China

<sup>3</sup> University of Chinese Academy of Science, Beijing 100049, China

**Citation:** Wang DW, You Y, Liu JF, et al. (2023) Impact pressure of debris flow on beam dam. Journal of Mountain Science 20(10). <https://doi.org/10.1007/s11629-023-8099-1>

© Science Press, Institute of Mountain Hazards and Environment, CAS and Springer-Verlag GmbH Germany, part of Springer Nature 2023

**Abstract:** The use of open-type check dams in mountainous areas has become common practice in order to mitigate the effects of debris flow and extend the service life of engineering structures. The beam dam, a common debris flow control system, has received less attention in research on the impact process of debris flow and check dams compared to solid check dams. Additionally, the estimation of impact pressure in debris flow primarily considers debris flow characteristics, without taking into account the influence of geometric characteristics of the transmission structure. To better understand the impact process of debris flow on beam dams, a series of small-scale debris flow impact tests were conducted in a model flume. Key parameters, including velocity, depth, and impact pressure, were measured. The results show that the maximum impact pressure of debris flow is affected by both the characteristics of the debris flow and the relative opening size of the beam dam. Due to flow and edge occlusion in the middle of the beam dam, the discharge of debris flow is enhanced, resulting in a longer impact process and

higher maximum impact pressure. Based on these findings, a calculation model of the maximum impact pressure of debris flow at the midpoint of the middle beam is proposed, which can be used to estimate the impact of debris flow on the discharge part of the beam dam.

**Keywords:** Debris flow; Beam dam; Impact pressure; Relative opening size; Calculation model

### 1 Introduction

Multiple types of debris flow dams are commonly constructed along debris flow channels to mitigate hazardous debris flows (Baldwin et al. 1987; VanDine, 1996; Hübl and Fiebiger, 2005; Chen et al. 2015; Wei et al. 2017; Kattel et al. 2018; Poudyal et al. 2019; Fang et al. 2023). Slotted dams are one of the major types of open-type check dams characterized by both trapping and discharging of large particles in debris flow, which changes the complete trapping of a solid gravity dam into a partial trapping. Compared with other types of check dams, the slotted dam structure mainly comprises vertical piles and crossbeams. This

**Received:** 04-May-2023  
**1<sup>st</sup> Revision:** 25-Jun-2023  
**2<sup>nd</sup> Revision:** 14-Aug-2023  
**3<sup>rd</sup> Revision:** 20-Sep-2023  
**Accepted:** 09-Oct-2023

structure has a higher opening rate that enables efficient discharge of sediment, fine gravel, and free water from the fluid, enabling the debris flow entering the dam reservoir to reach the separation of water and rock faster. Moreover, the structure of slotted dam is simple, convenient, and economically constructed, easy to maintain and manage, and is gradually widely used in debris flow prevention and control engineering in China and abroad. The beam dam, the most typical type of slotted dam, can greatly reduce water pressure on the dam, regulate the material composition of the debris flow, effectively improve storage capacity utilization, and extend the dam's service life due to its large opening size and good transmissibility. Examples of a typical beam dam are shown in Fig. 1.



**Fig. 1** (a) Typical beam dam in Nuorilang gully, Jiuzhaigou, Northwestern Sichuan, China; (b) Typical beam dam in Lalahu gully, Wenchuan, Northwestern Sichuan, China.

Since the abutment and support piers of the beam dam are primarily composed of high-strength reinforced concrete with large cross section, the debris flow's impact on these parts is relatively minimal. The beam of the dam structure regulates debris flow and is usually comprised of reinforced concrete or steel rails. To ensure a large opening ratio, the cross-section design size of the beam is often

small, resulting in weak structural strength, making it more prone to damage from debris flow impacts than other dam types. Additionally, due to the continuous and dynamic nature of debris flow, precast concrete beams often suffer abrasion damage or direct fractures, while steel rail beams mainly experience brittle fracture or bending deformation (refer to Fig. 1b). Nevertheless, the structural forms of existing beam dams vary significantly, and their design processes often rely on previous engineering experience. The mechanism and mode of beam dams in resisting the impact of debris flow remain unclear, and the spatiotemporal distribution characteristics of the maximum impact pressure of debris flow on the beam are not adequately understood. Furthermore, the calculation method of maximum impact pressure of the beam structure is imprecise.

Most current methods for calculating the impact pressure of debris flow utilize a one-dimensional dynamic model (Armanini et al. 2011; Hubl and Holzinger 2003):

$$P_{\max} = K\rho v^2 \quad (1)$$

where,  $P_{\max}$  is the impact pressure of debris flow (kPa),  $K$  is the empirical coefficient of impact pressure,  $\rho$  is the bulk density of debris flow ( $t/m^3$ ), and  $v$  is the velocity of debris flow (m/s). According to previous research and field observations, the empirical impact pressure coefficient ranges from 0.2 to 18.6 (Hung et al. 1984; Hübl and Holzinger 2003; Hu et al. 2011; Scheidl et al. 2013; Cui et al. 2015). The  $K$  coefficient is used to account for flow composition, blocking type, impact mechanism, and uncertainties in the natural environment (Song et al. 2017). It is worth noting that the values of  $K$  vary depending on the discharge and motion patterns that may be affected by the opening size and location of the beam dam.

In terms of model tests, Shieh's experiments in 2008 demonstrated that the impact pressure of debris flow with the same properties (material and velocity) on three different shaped dams (vertical, inclined, and curved) was significantly different, indicating that the impact pressure of debris flow is closely related to the structure of the dam. However, the early impact tests of debris flow did not measure the dynamic impact pressure due to sensor limitations (Shieh et al. 2008). Ng et al. (2016) conducted an experiment in which a debris flow trough was set up in the centrifuge, and the difference in impact pressure between rigid and flexible dams was studied. The experimental results show that the impact force of debris flow is notably

affected by the content and interaction between coarse particles (Ng et al. 2016). Additionally, Wei (1996) measured the impact pressure of debris flow on a solid check dam in laboratory tests, showing that the impact pressure of debris flow increased with the flow velocity (Wei et al. 1996).

Previous laboratory tests have mainly focused on the influence of the shape characteristics of solid check dams on the impact process of debris flow. However, there has been a lack of research on the impact process of open-type check dams, such as beam dams. In addition, studies on the impact of debris flow in beam dams are seldom analyzed in combination with the flow process of debris flow. The influence of the flow process of debris flow on the temporal and spatial distribution characteristics of the impact pressure is still unclear, and the existing calculation method only considers the flow properties of debris flow and does not consider the influence of the flow pattern change after the interaction between debris flow and beam dam on the maximum impact force of debris flow, so the calculation method of the maximum impact pressure is not accurate enough.

Therefore, this paper aims to study the impact process and the temporal and spatial distribution characteristics of the impact pressure of the beam dam through model tests. Finally, it will explore the calculation method of the maximum impact pressure at the middle point of the beam. This research is of great significance in ensuring the structural safety of beam dams, rationally utilizing engineering materials, optimizing structural design, prolonging the service life of the dam, and improving the application rate of beam dams in prevention and control engineering practice.

## 2 Material and Methods

### 2.1 Scaling principle

The Froude number of debris flow in nature may be relatively small. For example, the measured Froude

number of debris flow in Jiangjia Ravine falls between 1.5 and 2.0 according to Hu et al. (2011). Hübl (2005, 2009) believed that the Froude number of debris flow in flume tests often exceeds that in real debris flow ( $Fr < 3$ ), thus leading to an incorrect estimation of debris flow impact pressure. Therefore, it is essential to study the impact pressure of debris flow across a wider range of Froude numbers.

Based on a series of small-scale flume tests, Hübl and Holzinger (2003) discovered that the empirical impact pressure coefficient  $K$  ranged between 0.1 to 3.9 and is dependent on the Froude number of debris flow. Furthermore, they created a scale-independent formula to forecast the maximum impact pressure of debris flows:

$$P_{\max} = (4.5Fr^{-1.2})\rho v^2 \quad (2)$$

Froude number  $Fr$  dictates the behavior of fluid flow at a macro level. It is frequently employed to discern whether debris flows are influenced by inertia or gravity, as noted by both Hübl et al. (2009) and Choi et al. (2015). Moreover, it is extensively utilized to characterize the motion state of debris flow.

In this study, the values of  $Fr$  are set in the range of 3.79 to 7.70. These values align with the range of  $Fr$  values observed in field debris flow events, which fall between 0.45 and 13.00, as reported in previous studies (McArdell et al. 2007; Hübl et al. 2009; Kwan et al. 2015; Zhou et al. 2019). Table 1 presents the Froude number values extracted from prior research on debris flow and structural impact.

### 2.2 Test setup

The test equipment shown in Fig. 2 comprises a flume, a laser distance measuring instrument, a camera, and a data acquisition instrument. Specifically, the flume includes a tank (dimensions of 30cm × 50cm × 80cm) designed to store debris flow material, a generalized channel (dimensions of 400cm × 20cm × 30cm, with a variable slope of 0°-20°), and a recycle pool (dimensions of 80cm × 80cm

**Table 1** Summary of Froude number  $Fr$  for estimating debris flow impact pressure.

Structure type	Flow type	Froude number $Fr$	Data source
Solid dam	Dry sand	4.10-5.90	Ng et al. (2016)
	Viscous debris flow	3.20-3.90	
Single pile	Viscous debris flow (No coarse particles)	2.50-5.90	Cui et al. (2015)
Solid dam	Coarse flow and fine flow	1.20-13.00	Hübl and Holzinger (2003)
Single pile	Viscous debris flow in Jiangjia Ravine, China.	1.50-3.00	Hu et al. (2011)
Slit dam	A mixture of glycerin with glass beads and pebbles	2.47-0.51	Hu et al. (2020)



× 20cm) used for the recovery and reuse of debris flow. Regarding observation equipment, three high-definition cameras are used to record the entire process of debris flow movement during testing, with one positioned at a top view, one at a side view and the last one at a front view. Two laser distance measuring instruments are placed upstream and downstream of the beam dam to record the real-time change of mud level in the debris flow.

The beam dam used in the experiment is made of steel plates. The model's dimensions measure 200mm in width and 120mm in height, with 15 mm-wide columns positioned on the left and right sides, and a 170 mm-wide discharge section in the middle. The model is located 2.5m from the tank's outlet. Fig. 3a illustrates the opening size *b* of 20mm, which generally represents the typical opening form and structure of a beam dam in the field. Regarding sensor placement, each beam includes an impact pressure sensor in the middle of the beam, with three impact pressure sensors distributed across the three beams. The three impact pressure sensors are named A, B, and C from the bottom to the top along the central axis of the beam dam. Fig. 3b illustrates the sensor placement.

**2.3 Test material**

The material used in this test was taken from original samples collected from the debris flow accumulation area of Gangou in Longmenshan town, Pengzhou City. To minimize potential boundary effects on flume test results, coarse gravel with a diameter greater than 20mm was selectively removed, retaining only the original debris flow with a diameter less than 20mm. Particles with a size below 0.25mm were calibrated using a Mastersizer 2000 laser particle size analyzer. The grading curve of the test material is illustrated in Fig. 4. Following test requirements, debris flow soil samples were sifted for large particles, and the debris flow with initial bulk densities of 1.60t/m<sup>3</sup>, 1.80t/m<sup>3</sup> and 2.00t/m<sup>3</sup> was prepared according to different water content (39.8%, 28.6% and 19.7%). The amount of material in one test is 20L. In order to ensure the stability of the debris flow movement process, debris flow material in the tank were continuously and fully stirred, and a gate was used to control the stable discharge of debris flow material.

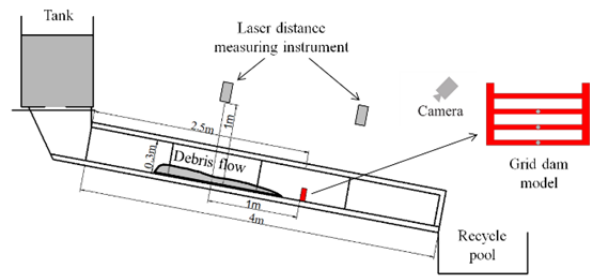


**Fig. 2** Experimental equipment.

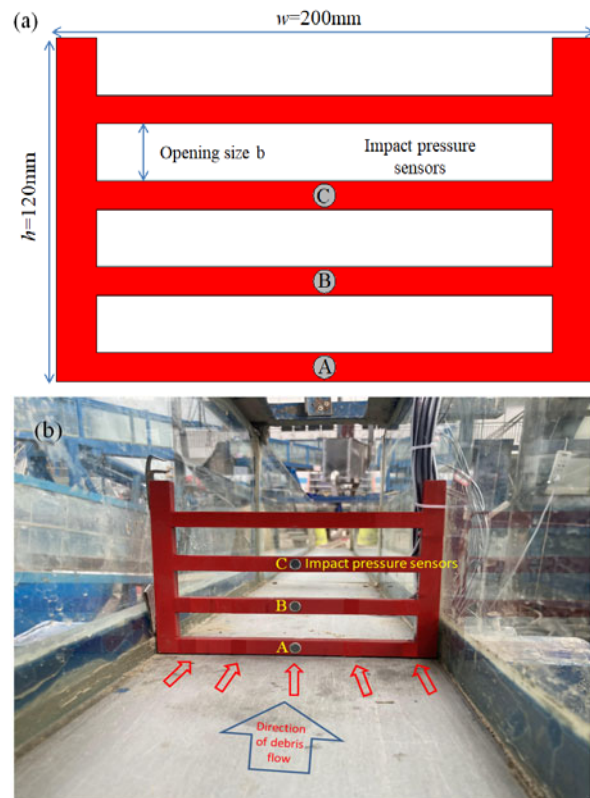


**Fig. 3** (a) Sensors layout of beam dam model; (b) Position relationship between beam dam model and channel.

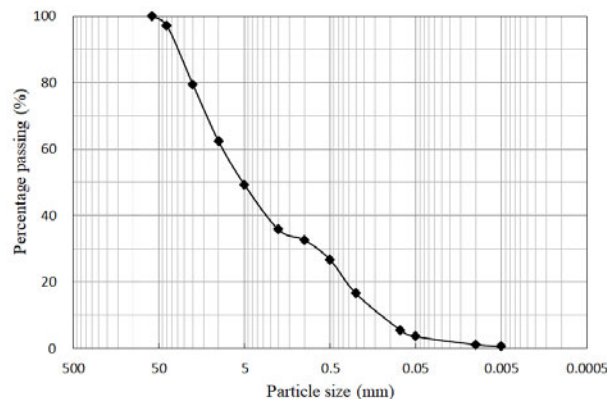


**Fig. 4** Particle size of debris flow material.

### 2.4 Test system

Real-time recording of velocity, depth, and impact of debris flow was conducted during the experiment. The impact pressure measurement system comprises 3 impact pressure sensors, a data acquisition instrument, and a laptop (Fig. 5a). The DY4100 impact pressure sensor has a range of 200kPa, a diameter of 8mm, a precision of  $\pm 0.25\%$ F.S., and a sampling frequency of 2000 Hz (Fig. 5b). This sensor is utilized to collect dynamic impact signals generated by debris flow acting on the beam dam. Furthermore, two laser distance measuring instruments (sampling frequency 20Hz, measuring accuracy 1mm) are used to capture the continuous change of mud depth when the debris flow passes through. Three high-definition cameras (sampling frequency 120Hz) were installed overhead and on the side of the water trough to record the flow of debris within the trough. Images back analysis was then utilized to obtain the average surface velocity and flow pattern. The surface velocity

of debris flow is interpreted by measuring the time of debris flow passing through fixed spacing sections.

### 2.5 Tests and Signal Processing

#### 2.5.1 Tests

A total of 45 tests were conducted to investigate the effects of changing the relative opening size, debris flow bulk density, and flume slope. Table 2 shows 45 test parameter groups with slopes of 4°, 6°, and 8°. To ensure the accuracy and reliability of the collected data, control groups were set under each test condition combination, including a no dam and solid dam group. The relative opening size of the beam dam indicates the passing ability of the beam dam, which can be expressed as  $b/d_{max}$ , where  $d_{max}$  represents the maximum particle size in the debris flow. The relative opening sizes of the beams are 0.75, 1.00, and 1.25, while the flume slopes are 4°, 6°, and 8°, and the bulk densities of debris flow are 1.60t/m<sup>3</sup>, 1.80t/m<sup>3</sup>, and

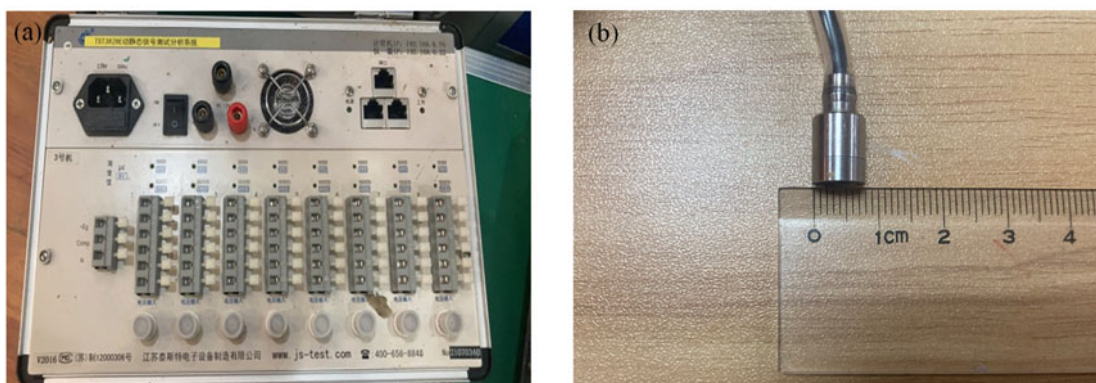


Fig. 5 (a) Data acquisition system; (b) Micro pressure sensor.

Table 2 Tests and fluid properties (4°, 6°, and 8° are slope angles of the flume).

Test ID	Relative opening size $b/d_{max}$	Bulk density $\rho$ (t/m <sup>3</sup> )	Approach velocity, $v$ (m/s)			Flow depth, $h$ (m)			Froude number, $Fr$		
			4°	6°	8°	4°	6°	8°	4°	6°	8°
1-3	0.75	1.60	3.72	4.80	5.56	0.048	0.048	0.057	5.42	7.00	7.44
4-6	1.00	1.60	3.66	4.82	5.26	0.050	0.052	0.055	5.23	6.75	7.16
7-9	1.25	1.60	3.52	4.32	5.06	0.049	0.055	0.057	5.08	5.88	6.77
10-12	No dam	1.60	3.61	4.62	5.12	0.047	0.050	0.055	5.32	6.60	6.97
13-15	Check dam	1.60	3.65	4.67	5.20	0.048	0.055	0.051	5.32	6.36	7.36
16-18	0.75	1.80	3.54	5.50	5.50	0.055	0.052	0.061	4.82	7.70	7.11
19-21	1.00	1.80	3.58	5.44	5.62	0.056	0.068	0.062	4.83	6.66	7.21
22-24	1.25	1.80	3.42	4.94	5.40	0.060	0.057	0.063	4.46	6.61	6.87
25-27	No dam	1.80	3.44	5.12	5.51	0.060	0.053	0.062	4.49	7.10	7.07
28-30	Check dam	1.80	3.50	4.98	5.36	0.055	0.060	0.059	4.77	6.49	7.05
31-33	0.75	2.00	3.66	5.28	5.58	0.070	0.068	0.060	4.42	6.47	7.28
34-36	1.00	2.00	3.56	5.30	5.58	0.064	0.065	0.055	4.50	6.64	7.60
37-39	1.25	2.00	3.18	5.14	5.50	0.072	0.066	0.061	4.79	6.39	7.11
40-42	No dam	2.00	3.26	5.32	5.65	0.068	0.070	0.063	3.99	6.42	7.19
43-45	Check dam	2.00	3.32	5.06	5.50	0.067	0.067	0.058	4.10	6.24	7.30

2.00t/m<sup>3</sup>. To analyze the dynamic characteristics of debris flow before impact, the approach velocity of debris flow was measured by float method, and the depth of debris flow was measured by laser distance measuring instruments. Moreover, this provides the *Fr* (Froude number) that reflects the hydrodynamic characteristics of the debris flow (Table 2).

### 2.5.2 Signal processing

To simplify the study, the impact pressure of debris flow was considered as continuous dynamic impact pressure. The original signal included noise from the measurement system, external interference, and sensor vibration caused by the impact process. To illustrate, the impact signal of the center point B of the middle beam under the test condition ( $\rho=1.80\text{t/m}^3$ , the slope is  $6^\circ$ ,  $b/d_{\max}=1$ ) was taken as an example. The original impact signal and the filtered impact signal are displayed in Fig. 6 to demonstrate the effect of the filtering process.

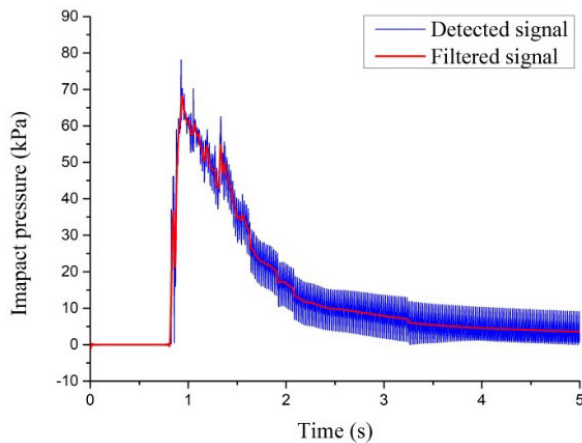


**Fig. 6** Original signal and the filtered signal of debris flow impact pressure of point B.

## 3 Experimental Results and Analysis

### 3.1 Impact process in the middle of the beam

Fig. 7 shows the time history and distribution of impact pressure at each point in the middle beam of the beam dam under typical test conditions, where the debris flow bulk density is  $1.80\text{t/m}^3$ , the flume slope is  $6^\circ$ , and the relative opening size  $b/d_{\max}$  is 1. Based on the analysis of debris flow movement on the beam dam, the impact process of debris flow can be divided into four stages:

Stage 1 (contact stage): The debris flow moves

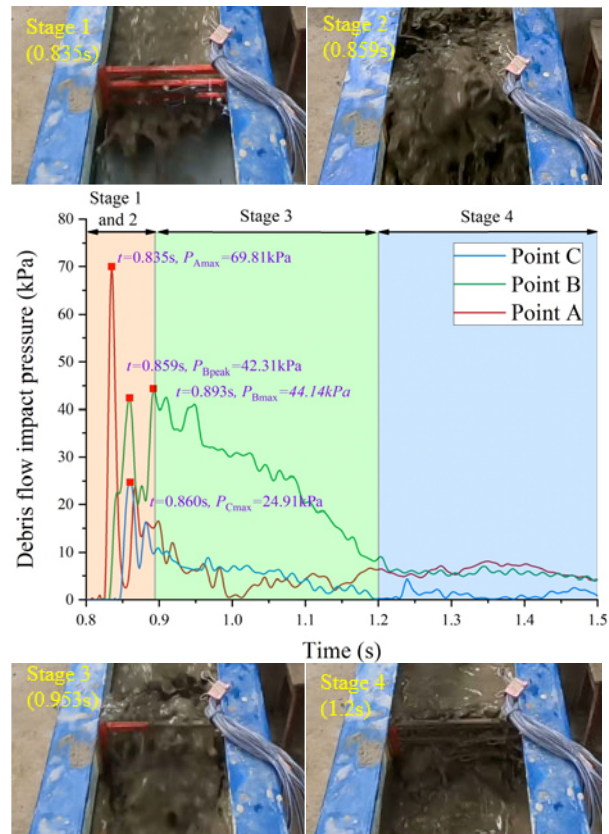


**Fig. 7** Time history curve of debris flow impact pressure at each measuring point in the middle of the beam (Test conditions:  $\rho=1.80\text{ t/m}^3$ , the slope is  $6^\circ$ ,  $b/d_{\max}=1$ ).

steadily in the flume towards the oncoming surface of the beam dam from the tank. The sensor at the bottom detects the impact pressure first. This stage lasts approximately 0.83 seconds.

Stage 2 (runup stage): Upon interaction, the debris flow rapidly climbs vertically along the beam dam. Impact pressure values of the three beams within the debris flow increase significantly and first peak appears in chronological order. The first peak impact pressures are detected at points A, B and C at 0.835s, 0.859s and 0.860s respectively. Subsequently, due to the impact of the debris, the impact force at point A is rapidly reduced as a result of the rapid deceleration of the debris. The impact force at point C is also reduced with the reduction of the runup height at the dam, and the impact force at point B begins to enter the next stage after reaching a second peak impact force at 0.893s. Based on the test results, we find that the maximum impact force at point B occurs at the second peak impact force of 44.14kPa. Compared with the first peak impact force (42.31kPa), the time lag is 0.024s. As the debris flow continues to



accumulate along the edge and bottom of the beam dam, there is a continuous increase in the quantity of debris flow in the middle of the beam dam, resulting in a hysteresis effect in the maximum impact pressure.

Stage 3 (crossing stage): Debris flow crossing in the beam dam can be classified into two types; crossing between the beams and the top of the dam. Due to the discharge effect and decreasing velocity of the incoming flow, debris flow begins to gradually accumulate behind the dam, resulting in a decrease of impact pressure on each measuring point. The damping process demonstrates a trend of shock decline, which lasts for about 0.3 seconds. In this stage, the impact force of measuring point B is obviously greater than that of the other two measuring points, which may be caused by the continuous discharge of debris flow at measuring point B. The impact force of measuring point A quickly changes into static pressure due to the occlusion of measuring point A, while the impact force of measuring point C, which is higher than the depth range of debris flow, no longer fluctuates after the debris flow falls down.

Stage 4 (accumulation and discharge stage): Debris flow impact pressure reduces rapidly from the flood peak value of the previous stage. However, the decline rate is noticeably slower than that of the preceding stage. Over time, the discharge effect between the beams decreases gradually, and the impact pressure acting on each measuring point transforms slowly into a static pressure load. Subsequently, a stable state is reached from the bottom to the top, which occurs approximately at 1.2s.

### 3.2 Variation characteristics of maximum impact pressure

Test results show that the bulk density of debris flow, the relative opening size of the beam dam and the slope of the flume are the main factors affecting the maximum impact pressure in the middle of the beam dam.

#### 3.2.1 Bulk density of debris flow

Based on the test results, the maximum impact pressure in the middle of the beam dam is significantly influenced by the bulk density (Fig. 8a). Specifically, when the bulk density of debris flow is 1.60t/m<sup>3</sup>, the maximum impact pressure  $P_{max}$  of debris flow occurs mainly at the bottom beam and gradually decreases from bottom to top along the

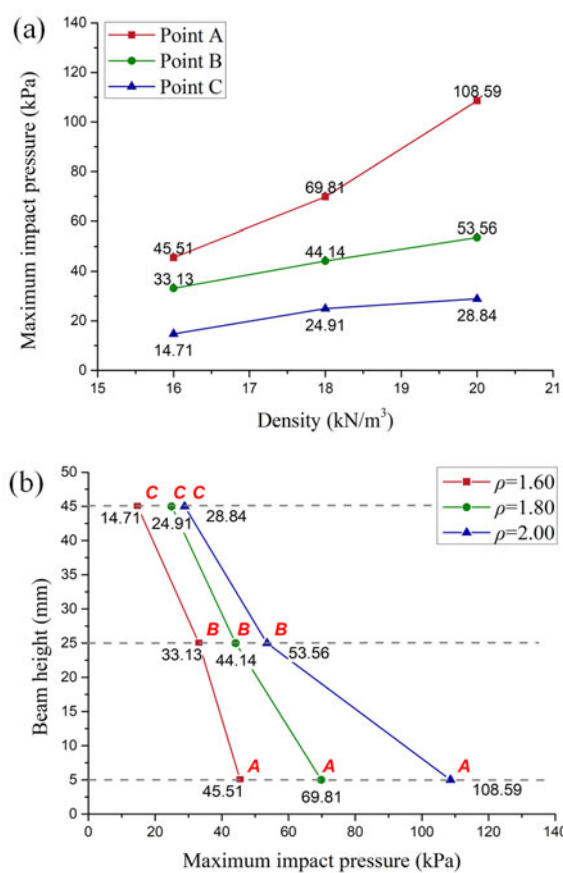


**Fig. 8** (a) Variation trend of maximum impact pressure at the middle point of the beam under bulk density variation; (b) Longitudinal distribution of maximum impact pressure under bulk density variation (Test conditions:  $b/d_{max}=1$ , the slope is 6°).

depth direction. This means that the maximum impact pressure of debris flow with low bulk density increases along the longitudinal height of the beam and gradually decreases. Furthermore, low bulk density debris flow with low solid components content implies poor integrity and is more prone to passing through the bottom of the beam dam, hence yielding little difference in maximum impact pressure values at different heights in the middle of the beam (Fig. 8b). In contrast, when the bulk density of debris flow is 2.00t/m<sup>3</sup>, the maximum impact pressure value is higher than that under the low bulk density condition. At this stage, the maximum impact pressure  $P_{max}$  of debris flow appears at the bottom measuring point A, with a value of 105.59kPa. The maximum impact pressure at the top measuring point C, however, is relatively low, with a value of only 28.84kPa. This indicates that the higher the solid content in the debris, the higher the momentum of a more cohesive material.



### 3.2.2 Relative opening size

Three different relative opening sizes of the beam dam were selected for analysis. Fig.9a displays the relationship between the relative opening size and the maximum impact pressure at each measuring point in the middle of the beam.

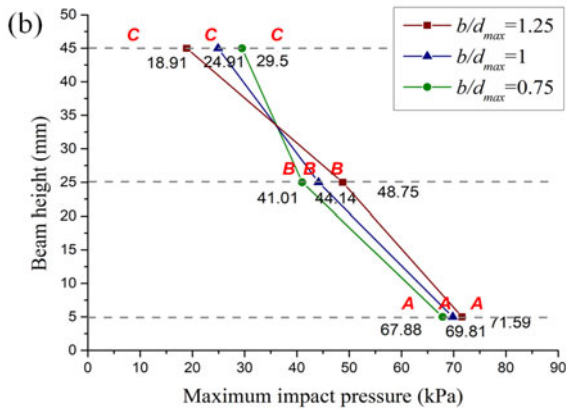
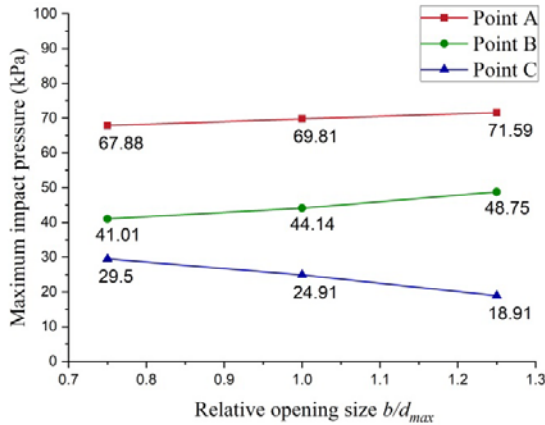


**Fig. 9** (a) Variation trend of maximum impact pressure at the middle point of the beam under relative opening size variation; (b) Vertical distribution of maximum impact pressure under relative opening size variation (Test conditions:  $\rho=1.80 \text{ t/m}^3$ , the slope is  $6^\circ$ ).

Generally, as the relative opening size increases, the trend of the maximum impact pressure at the midpoint of the beam becomes distinctively different. The maximum impact pressure at measuring point A remains basically unchanged. This may be because the depth of measuring point A remains constant, always located in the range of mud depth. As the relative opening size increases, the maximum impact pressure at measuring point B shows a clear upward trend. This may be attributed to the increased discharge efficiency of debris flow through the opening between the bottom beam and the middle beam, leading to a slower blocking process. As the blockage develops, the quantity of debris flow

abruptly increases at measuring point B. Therefore, the maximum impact pressure often lags behind the peak impact pressure generated by the debris flow head. The maximum impact pressure at measuring point C decreases significantly with an increase in the relative opening size. This indicates that the higher the measuring point C and the wider the relative opening size, the easier it is for the debris flow to discharge from the bottom opening, making it more challenging for the debris flow head to reach the measuring point C. Consequently, the maximum impact pressure generated at the measuring point C will be smaller and smaller (Fig. 9b).

### 3.2.3 Slope

The test results indicate that the maximum impact pressure in the middle of the beam increases as the slope of the flume increases (as depicted in Fig. 10a). Moreover, the maximum impact pressure of debris flow gradually decreases from bottom to top along the longitudinal axis. As the slope becomes steeper, the maximum impact pressure on each measuring point in the middle of the beam significantly rises. Additionally, with the increasing height of the measuring point, the maximum impact pressure increases more notably. When the slope is small ( $\theta=4^\circ$ ), the velocity of the debris flow is relatively low and can be regarded as a plug flow with good integrity, and there is no clear water and stone splash in the running-up process. As a result, there is a relatively small difference in the impact pressure of each measuring point in the middle of the beam. However, when the slope is large ( $\theta=8^\circ$ ), the maximum impact pressure on each measuring point of the beam dam dramatically increases, with significant differences among the maximum impact pressure of each measuring point. The reason is that as the slope becomes steeper, the velocity of the debris flow significantly increases, leading to poor integrity. During the contact and climb stages, a violent rushing and climbing phenomenon occurs while the material composition of debris flow becomes nonuniform in the longitudinal direction. All these factors contribute to the clear variation in the maximum impact pressure of measuring point C which is relatively lower than that of measuring point A. In this instance, the maximum impact pressure on measuring point B is  $105.59\text{kPa}$ , while the maximum impact pressure on measuring point C at the top is  $35.91\text{kPa}$  (Fig. 10b).

### 3.3 Calculation method of maximum impact pressure

Based on the results of the flume tests, the process of debris flow discharge and blocking at the bottom beam is not affected by the change in the relative opening size. Instead, it is only affected by the bulk density of debris flow and the slope of the flume. Hence, the maximum impact pressure at the bottom beam is still calculable using the previous impact pressure formula, regardless of the relative opening size. Since the top beam is located where the debris flow rises and climbs, it cannot endure the continuous impact of debris flow. Therefore, the maximum impact pressure of debris flow at the top beam is random and can be predicted by calculating the maximum impact pressure of the middle beam. However, the maximum impact pressure of the middle point B of the middle beam is not only dependent on the nature of debris flow but also influenced by the change of the relative opening size. As the relative opening size increases, the maximum impact pressure also shows an upward trend. We believe that the maximum impact pressure of middle point B is mostly affected by the velocity  $v$ , bulk density  $\rho$ , debris flow and maximum debris flow particle size  $d_{max}$ , beam dam opening size  $b$ , the slope of flume  $\theta$  and the acceleration of gravity  $g$ . To simplify the analysis, we can express the maximum impact pressure of the middle point B as:

$$P_{Bmax} = f(v, \rho, g, b, d_{max}, \theta) \quad (3)$$

Following the principle of dimensional analysis, the given equation consists of six variables, out of which three factors can be considered as basic variables as per the  $\pi$  theorem. Applying the principle of dimensional consistency, Eq. (3) can be simplified as:

$$\frac{P_{Bmax}}{\rho v^2} = f\left(\frac{gh}{v^2}, \frac{d_{max}}{b}, \theta\right) \quad (4)$$

Further, the empirical coefficient of impact pressure of the middle point B  $K_B$  can be written as:

$$K_B = f\left(\frac{gh}{v^2}, \frac{d_{max}}{b}, \theta\right) \quad (5)$$

Drawing upon the previous analysis, it can be inferred that the empirical coefficient of impact pressure  $K_B$  is influenced not only by the Froude number  $Fr$  but also by the relative opening size  $b/d_{max}$ , representing the discharge effect of debris flow at the

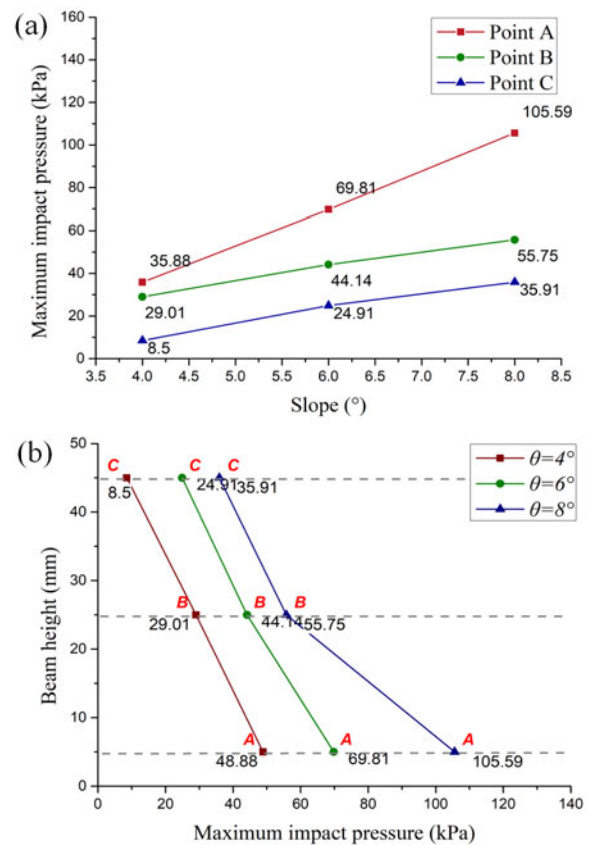


**Fig. 10** (a) Variation trend of maximum impact pressure at the middle point of the beam under slope variation; (b) Longitudinal distribution of maximum impact pressure under slope variation (Test conditions:  $\rho=1.80 \text{ t/m}^3$ ,  $b/d_{max}=1$ ).

beam dam.

By general convention, the Froude in the above equation is:

$$Fr = \frac{v}{\sqrt{gh \cos \theta}} \quad (6)$$

The empirical coefficient of impact pressure of the middle point B can be simplified as:

$$K_B = f\left(\frac{gh}{v^2}, \frac{d_{max}}{b}, \theta\right) = f_1(Fr) \cdot f_2\left(\frac{b}{d_{95}}\right) \quad (7)$$

The empirical coefficient  $K_B$  of debris flow at a beam dam under varying bulk density conditions is depicted for different Froude numbers  $Fr$  in Fig. 11a. Additionally, the empirical coefficient  $K_B$  under different relative opening sizes  $b/d_{max}$  is illustrated in Fig. 11b. It is evident that the empirical coefficient  $K_B$  decreases with an increase in Froude number  $Fr$  and increases with an increase in relative opening size  $b/d_{max}$ . This highlights that relative opening size plays a key role in the discharge and blocking mechanism of

debris flow. Moreover, a larger relative opening size results in a longer discharge duration of debris flow at the midpoint beam.

Through the fitting analysis of experimental data, the expression of the impact pressure coefficient of debris flow can be written as follows:

$$K_B = 4.2839 Fr^{-0.7867} \cdot \left(\frac{b}{d_{max}}\right)^{0.1215} \quad (8)$$

Therefore, the maximum impact pressure of debris flow at the middle point B can be expressed as:

$$P_{Bmax} = \left(4.2839 Fr^{-0.7867} \cdot \left(\frac{b}{d_{max}}\right)^{0.1215}\right) \rho v^2 \quad (9)$$

As illustrated in Fig. 12, a comparison between the maximum impact pressure measured and the maximum impact pressure calculated demonstrates that the equation's accuracy is dependable.

#### 4 Discussions

In this paper, we carried out small flume tests to measure the impact pressure of debris flow on a beam dam. To filter and denoise the detected impact signal, we utilized wavelet analysis. By analyzing the flow process of debris flow, we studied in detail the impact process and the temporal and spatial distribution characteristics of the impact pressure of debris flow at the beam dam. Finally, we established a calculation method for the maximum impact pressure at the midpoint B. Furthermore, we discussed the relationship between the longitudinal distribution characteristics of debris flow impact load and impact failure characteristics.

##### 4.1 Test results are reliable

Our tests have revealed that typical debris flow impact processes can be observed under different combinations of test conditions. The observed impact processes are consistent with the records of debris flow events in Jiangjia Ravine. Previous studies have shown that the dynamic pressure of debris flow is 18-60 kPa when the flow velocity in Jiangjia Ravine is 5-10 m/s (Hu et al. 2011). This is in good agreement with our experimental records at the same flow velocity. In order to obtain more accurate data on the overall impact pressure of debris flow, this paper does not consider the impact load caused by large particles

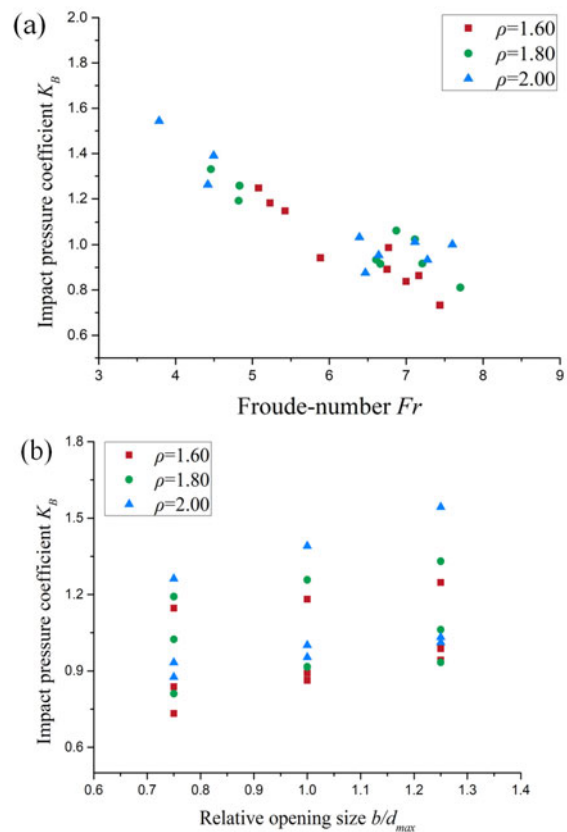


**Fig. 11** (a) Relationship between Froude number  $Fr$  and the empirical coefficient of impact pressure  $K_B$ ; (b) Relationship between the relative opening size  $b/d_{max}$  and the empirical coefficient of impact pressure  $K_B$ .

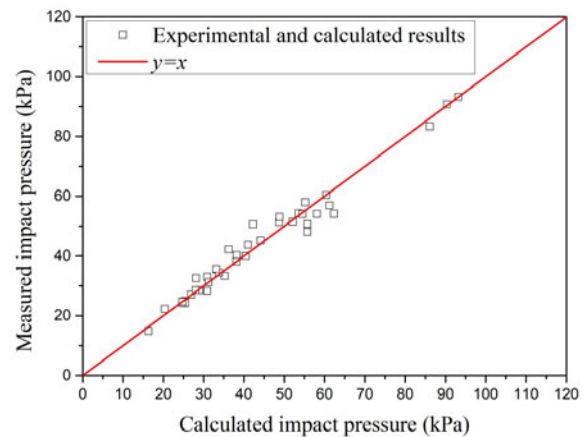


**Fig. 12** Comparison between the measured and calculated maximum impact pressures.

of debris flow. This is because the impact signal caused by large particles is random, which makes it difficult to analyze the change process of the overall impact pressure of debris flow and obtain the maximum impact pressure. However, it should be noted that large particles may cause more significant damage to the beam (Hung et al. 1984; Chen and Tang

2006). In this paper, we focused on the overall impact pressure of debris flow and analyzed the distribution characteristics of the maximum impact pressure. Overall, our tests are reliable and provide valuable insights into the impact of debris flow on beam dams.

#### 4.2 Impact pressure calculation model is improved

Previous studies have shown that the empirical coefficient of impact pressure is primarily influenced by the Froude number. The Froude number is used to describe the flow patterns of debris flow, while the relative opening size of a beam dam is used to describe the discharge process of debris flow at the beam dam, which in turn allows for the model similarity of small flume tests. During our tests, the Froude numbers ranged from 3.79 to 7.70, which were consistent with the Froude numbers obtained from field observation events of debris flow (ranging from 0.45 to 13.00) (McArdell et al. 2007; Hübl et al. 2009; Kwan et al. 2015; Zhou et al. 2019). The changing trend of the impact coefficient and Froude number obtained in our experiments is consistent with previous research results (Fig. 13). Furthermore, under the same Froude number conditions, the impact coefficient obtained in our experiments was slightly larger than that obtained in other studies (Proske et al. 2010; Scheidl et al. 2013; Zhang and Yuan 1985; Hübl and Holzinger 2003; Tiberghien et al. 2007; Cui et al. 2015). This may be because the blockage and discharge process at the opening between the beams affects the impact process of the debris flow at midpoint B. As mentioned in the

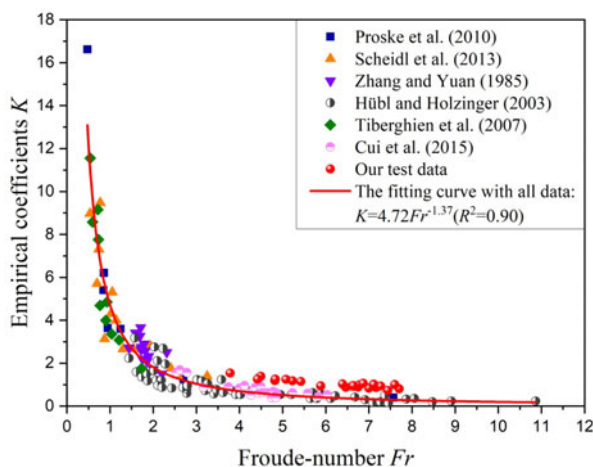


**Fig. 13** Relationships between Froude number and the empirical coefficients.

previous analysis, the maximum impact pressure at the midpoint E of the beam does not appear at the first peak value, but rather at a later peak value that is slightly larger than the first one. This indicates that considering the influence of the relative opening size on the maximum impact force of the debris flow can make the calculation of the maximum impact force at the midpoint B of the beam more accurate.

#### 4.3 Vulnerable parts of the beam can be better judged

The damaging effect of debris flow on a beam dam can be described as follows: the strong impact of the debris flow head on the base of the beam dam leads to structural damage (Fig. 14a). As the debris flow continues to accumulate at the base, it slowly starts to damage the beam dam from bottom to top (Fig. 14b). During stage 1, the debris flow head comes into contact with the beam dam, and the size of the particles gradually increases from the top to the bottom of the longitudinal section of the flow. This results in a dynamic pressure that can be represented as a trapezoidal load, and the maximum impact pressure point is in point A. Consequently, the bottom beam is more likely to be damaged by the impact. During stage 2, the debris flow starts to form a stable discharge at the beam dam. At this moment, the impact load can be approximated as a uniform load, and the maximum impact pressure is basically consistent longitudinally. During stage 3, As the debris flow continues to accumulate along the edge and bottom of the beam dam, there is a continuous increase in the quantity of debris flow in the middle of the beam dam, and the maximum impact pressure of the debris flow appears at central point B, and the load distribution becomes roughly pentagon. During stage 4, the flow velocity decreases as the quantity of debris flow decreases. As such, the impact pressure of the debris flow on the beam dam gradually transforms into a static pressure. The static load distribution is triangular, and the maximum impact pressure point is located in point A (Fig. 15).

Many existing engineering designs only take into account the impact of the initial debris flow, but ignore the continuous impact process caused by blockages. This oversight tends to underestimate the risks associated with debris flow impact on the discharge area of the beam dam. Therefore, it is crucial to consider the impact process under constant influence to ensure



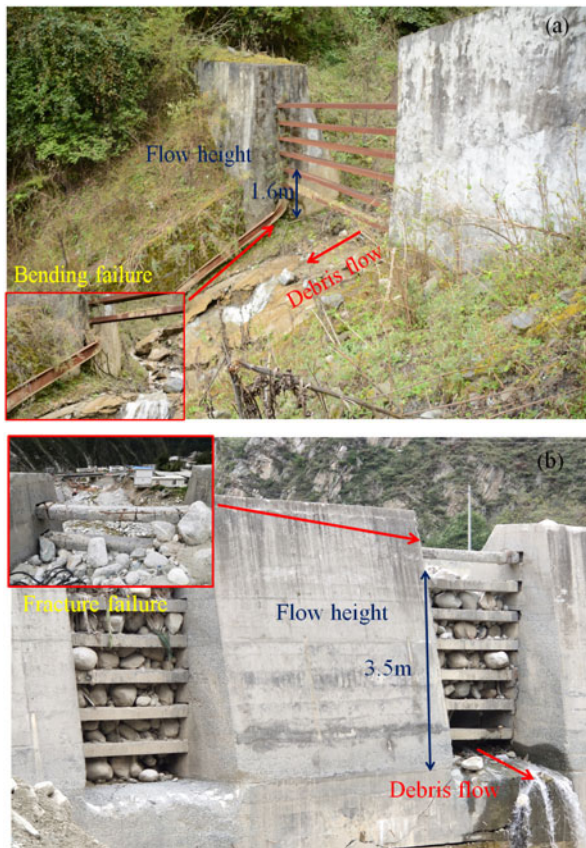


**Fig. 14** (a) Impact failure at the top of beam dam; (b) Impact failure at the bottom of beam dam.

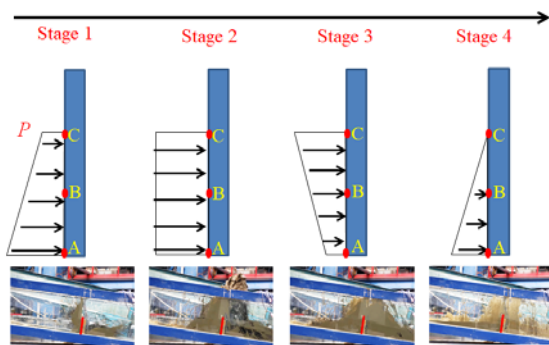


**Fig. 15** Simplified diagram of load distribution in debris flow impact process.

accurate risk assessments. Improving design considerations in this regard is paramount.

## 5 Conclusions

In this study, a series of flume tests were carried out under specific conditions to investigate the effects of relative opening size, bulk density of debris flow, and the flume slope on the maximum impact pressure

of debris flow on a beam dam. The following conclusions can be drawn based on the study:

(1) The impact process of debris flow on the beam dam can be divided into four stages: contact stage, climb stage, crossing stage, and storage and discharge stage. The peak impact pressure during the contact and climb stage is not influenced by the relative opening size, but rather dependent on the nature of the debris flow.

(2) The maximum impact pressure of debris flow at the middle point B is affected by the bulk density of debris flow, slope of the flume, and relative opening size. A larger relative opening size results in a longer debris flow discharge process in the middle of the beam dam. As the debris flow continues to accumulate along the edge and bottom of the beam dam, there is a continuous increase in the quantity of debris flow in the middle of the beam dam, resulting in a hysteresis effect in the maximum impact pressure.

(3) Based on the measured impact pressure data and dimensional analysis, a calculation model for the maximum impact pressure at the middle point B is proposed. Compared to traditional methods, the new model considers the influence of the debris flow discharge process on the maximum impact pressure, leading to a more secure impact resistance design for the vulnerable position of the beam structure.

(4) To simplify the analysis and establish a calculation model for the maximum impact pressure of debris flow, this paper does not consider the impact of boulders. However, in debris flow events that occur in the field, boulders often cause more significant damage to the beam dam. Therefore, it is necessary to further explore the impact of large blocks on the beam dam's impact pressure in future research. This could enhance the accuracy of the analysis and enable better predictions of the damage that debris flow events can cause.

## Acknowledgments

This study was jointly funded by the National Natural Science Foundation of China (Grant No.42201095) and the Natural Science Foundation of Sichuan (Grant No.2022NSFSC1032).

## Author Contribution

WANG Dong-wei: Investigation, Methodology, Visualization, Conceptualization, Formal analysis,

Writing-original draft, Writing-review & editing. YOU Yong: Supervision, Writing-review & editing. LIU Jin-feng: Writing-review & editing. SUN Hao: Funding curation, Writing-review & editing. WANG Zhuang: Investigation, Writing-review & editing.

## References

- Armanini A, Larcher M, Odorizzi M (2011) Dynamic impact of a debris flow front against a vertical wall. In: Proceedings of the 5th International Conference on Debris Flow Hazards Mitigation: Mechanics, Prediction and Assessment, Padua, Italy. pp 1041-1049. <https://doi.org/10.4408/IJECE.2011-03.B-113>
- Baldwin JE, Donley HF, Howard TR (1987) On debris flow/avalanche mitigation and control, San Francisco Bay area, California. *Rev Eng Geol* 223-236. <https://doi.org/10.1130/reg7-p223>
- Chen HK, Tang, HM (2006) Method to calculate impact force and impact time of two-phase debris flow. *China Journal of Highway and Transport* 19(3): 19-23. (In Chinese) <https://doi.org/10.1097/01.bpo.0000188995.29050.b9>
- Chen XQ, Cui P, You Y, et al. (2015) Engineering measures for debris flow hazard mitigation in the Wenchuan earthquake area. *Eng Geol* 194:73-85. <https://doi.org/10.1016/j.enggeo.2014.10.002>
- Choi CE, Ng CWW, Au-Yeung SCH, et al. (2015) Froude scaling of landslide debris in flume modelling. *Landslides* 12(6): 1197-1206. <https://doi.org/10.1080/1023697X.2015.1102658>
- Cui P, Zeng C, Lei Y (2015) Experimental analysis on the impact force of viscous debris flow. *Earth Surf Proc Land* 40(12): 1644-1655. <https://doi.org/10.1002/esp.3744>
- Fang K, Tang HM, Li CD, et al. (2023) Centrifuge modelling of landslides and landslide hazard mitigation: A review. *Geosci Front* 14(1). <https://doi.org/10.1016/j.gsf.2022.101493>
- Hu HS, Zhou GGD, Song DR, et al. (2020) Effect of slit size on the impact load against debris-flow mitigation dams. *Eng Geol* 274:105. <https://doi.org/10.1016/j.enggeo.2020.105764>
- Hu KH, Wei FQ, Li Y (2011) Real-time measurement and preliminary analysis of debris flow impact force at Jiangjia Ravine. *China. Earth Surf Proc Land* 36(9): 1268-1278. <https://doi.org/10.1002/esp.2155>
- Hübl J, Fiebigler G (2005) Debris-flow mitigation measures. In: *Debris-Flow Hazards and Related Phenomena*. Springer, Berlin Heidelberg. pp 445-487. [https://doi.org/10.1007/3-540-27129-5\\_18](https://doi.org/10.1007/3-540-27129-5_18)
- Hübl J, Holzinger G (2003) Development of bases for the dimensioning of canopy-open structures for bedload management in torrents: classification of torrent barriers. *WLS Report* 50. (In German)
- Hübl J, Suda J, Proske D (2009) Debris flow impact estimation. In: *Proceedings of the 11th International Symposium on Water Management and Hydraulic Engineering*, Ohrid, Macedonia. pp 1-4.
- Hungr O, Morgan GC, Kellerhals R (1984) Quantitative analysis of debris torrent hazards for design of remedial measures. *Can Geotech J* 21(4): 663-677. <https://doi.org/10.1139/t84-073>
- Kattel P, Kafle J, Fischer JT, et al. (2018) Interaction of two-phase debris flow with obstacles. *Eng Geol* 242:197-217. <https://doi.org/10.1016/j.enggeo.2018.05.023>
- Kwan JSH, Koo RCH, Ng CWW (2015) Landslide mobility analysis for design of multiple debris-resisting barriers. *Can Geotech J* 52(9):1345-1359. <https://doi.org/10.1139/cgj-2014-0152>

## Ethics Declaration

**Data Availability:** Data supporting this Research article are available from the corresponding author on request.

**Conflict of interest:** The authors declare no conflicts of interest.

- McArdell BW, Bartelt P, Kowalski J (2007) Field observations of basal forces and fluid pore pressure in a debris flow. *Geophys Res Lett* 34(7). <https://doi.org/10.1029/2006GL029183>
- Ng CWW, Song D, Choi CE, et al. (2016) Impact mechanisms of granular and viscous flows on rigid and flexible barriers. *Can Geotech J* 54(2):188-206. <https://doi.org/10.1139/cgj-2016-0128>
- Poudyal S, Cho CE, Song D, et al. (2019) Review of the mechanisms of debris flow impact against barriers. In: *Association of Environmental and Engineering Geologists; Colorado School of Mines. Arthur Lakes Library. Special publication* 28. <https://doi.org/10.25676/11124/173112>
- Proske D, Suda J, Hübl J (2011) Debris flow impact estimation for breakers. *Georisk: Assessment and Management of Risk for Engineered Systems and Geohazards* 5(2):143-155. <https://doi.org/10.1080/17499518.2010.516227>
- Scheidt C, Chiari M, Kaitna R, et al. (2013) Analysing Debris Flow Impact Models, based on a Small Scale Modelling Approach. *Surv Geophys* 34(1):121-140. <https://doi.org/10.1007/s10712-012-9199-6>
- Shieh CL, Ting CH, Pan HW (2008) Impulsive force of debris flow on a curved dam. *Int J Sediment Res* 23(2):149-158. [https://doi.org/10.1016/S1001-6279\(08\)60014-1](https://doi.org/10.1016/S1001-6279(08)60014-1)
- Song D, Zhou GGD, Xu M, et al. (2019) Quantitative analysis of debris flow flexible barrier capacity from momentum and energy perspectives. *Eng Geol* 251:81-92. <https://doi.org/10.1016/j.enggeo.2019.02.010>
- Tiberghien D, Laigle D, Naaim M, et al. (2007) Experimental investigations of interaction between mudflow and an obstacle. In: *International Conference on Debris-Flow Hazards Mitigation: Mechanics, Prediction, and Assessment*, Proceedings. pp 281-292.
- VanDine DF (1996) *Debris Flow Control Structures for Forest Engineering*. Research Branch, BC Ministry of Forests, Victoria, BC (Working paper 08/1996.75 pages)
- Wei H (1996) Experimental study on impact force of debris flow heads. *China Railway Science* 03: 50-62. (In Chinese) <https://doi.org/CNKI:SUN:ZGTK.0.1996-03-005>
- Wei ZL, Shang YQ, Li Q, et al. (2017) Application and design of an efficient siphon dewatering system for debris flow mitigation: a case study of a small catchment in Zhejiang Province, China. *Eng Geol* 226:146-160. <https://doi.org/10.1016/j.enggeo.2017.06.004>
- Zakeri A, Heg K, Nadim F (2009) Submarine debris flow impact on pipelines - Part II: Numerical analysis. *Coast Eng* 56(3): 384. <https://doi.org/10.1016/j.coastaleng.2008.06.003>
- Zhang SC, Yuan JM (1985) Impact force of debris flow and its detection. *Memoirs of Lanzhou Institute of Glaciology and Cryopedology, Chinese Academy of Sciences*. pp 269-274. (In Chinese)
- Zhou GGD, Hu HS, Song D, et al. (2019) Experimental study on the regulation function of slit dam against debris flows. *Landslides* 16(1):75-90. <https://doi.org/10.1007/s10346-018-1065-2>